Available online at www.sciencedirect.com
SCIENCE DIRECT®
Journal of Computational Physics 194 (2004) 233–255
JOURNAL OF COMPUTATIONAL PHYSICS
www.elsevier.com/locate/jcp

Anisotropic mesh adaptation for the solution of the Stefan problem

Youssef Belhamadia, André Fortin *, Éric Chamberland

GIREF, Département de mathématiques et de statistique, Université Laval, Bureau 2986, Pavillon Pouliot, Qué., Canada G1K 7P4

Received 11 June 2003; received in revised form 22 September 2003; accepted 22 September 2003

Abstract

A new finite element formulation for the solution of the classical Stefan problem is introduced. It is obtained by a slight modification of the phase-field formulation used for dendritic growth where both the phase-field ϕ and the temperature T are discretized. An anisotropic mesh adaptation strategy is also presented to further increase the accuracy of the method. Numerical results for two-dimensional examples illustrating the performance and accuracy of the proposed method are presented.
© 2003 Elsevier B.V. All rights reserved.

Keywords: Stefan problem; Phase change; Phase-field formulation; Finite element method; Hierarchical error estimator; Anisotropic mesh adaptation

1. Introduction

The classical two-phase Stefan problem can be used to model phase change in various applications. The two phases, typically solid and liquid, are separated by an interface (or free boundary) which is defined by the melting temperature T_f. The main difficulty in such simulations is to accurately compute this moving free surface where phase change occurs. Moreover, on this interface, an energy balance condition, often called the Stefan condition, must be imposed.

These difficulties were partly overcome by the introduction of the so-called enthalpy formulation. In this formulation, the interface is not explicitly computed and the energy balance condition is satisfied automatically. The reader is referred to Nochetto et al. [11] and to Fortin and Belhamadia [5] for a complete discussion.

As an alternative, the phase-field formulation was introduced for the solution of the modified Stefan problem where the Gibbs–Thomson interface condition is imposed (see [9] for instance). This condition

* Corresponding author. Tel.: +418-656-3489; fax: +418-656-3404.
E-mail address: afortin@giref.ulaval.ca (A. Fortin).

0021-9991/$ - see front matter © 2003 Elsevier B.V. All rights reserved.
doi:10.1016/j.jcp.2003.09.008

includes surface effects such as surface tension and undercooling and is more general than the Stefan condition.

The main focus of this study is to present an intermediate formulation between the enthalpy and phase-field formulations. In the phase-field model, two partial differential equations have to solved: one for the temperature and the second for the phase parameter ϕ which takes on constant values in the solid and liquid phases. For the classical Stefan problem the partial differential equation for ϕ can be replaced by an algebraic equation while the heat equation remains the same. This formulation simplifies the phase-field model and can be used when surface effects are neglected at the interface. For this reason the presented formulation is called a semi-phase-field model. The proposed formulation presents strong similarities with the phase-field relaxation model introduced in Jiang and Nochetto [6].

To further increase the accuracy of the numerical simulations, an adaptive remeshing method based on an approximation of a hierarchical error estimator is also introduced. As shall be seen, the adaptive method concentrates the elements in the vicinity of the freezing front allowing a better prediction of the interface position and form.

The layout of this paper is as follows: the Stefan problem is presented in the next section while the semi-phase-field model is described in Section 3. Section 4 is devoted to the description of the adaptive strategy and some numerical results showing the potential of the proposed formulation and adaptive strategy are presented in Section 5.

2. Stefan problem

From a numerical point of view, phase change problems require the solution of the heat conduction equation in a domain Ω consisting of solid and liquid phases Ω_s and Ω_l. The heat conduction equation must be solved in each phase while at the interface Γ, the temperature T (in K) is continuous and its value is the melting temperature T_f. Moreover, a heat balance equilibrium condition must also be enforced on Γ. The governing equations for multi-phase heat conduction problems have the form

$$\begin{cases} \rho_i c_i \frac{\partial T}{\partial t} - \nabla \cdot (\boldsymbol{K}_i \nabla T) = f_i & \text{in } \Omega_i, \ \ i = s, l, \\ T = T_f & \text{on } \Gamma, \\ (\boldsymbol{K}_s \nabla T) \cdot \boldsymbol{n}_s - (\boldsymbol{K}_l \nabla T) \cdot \boldsymbol{n}_l = \rho_l L V_\Gamma & \text{on } \Gamma. \end{cases} \tag{1}$$

The last equation is the energy balance (Stefan) condition. Subscripts s and l refers to the solid and liquid phases and the following symbols have been used: $\boldsymbol{K}_i$ is the thermal conductivity tensor (W/m K), ρ_i is the density (kg/m^3), c_i is the specific heat (J/kg K), f_i is a possible heat source, L is the latent heat of fusion (J/kg), V_Γ is the interface normal velocity (m/s).

The major difficulty in this problem is that the interface Γ is not known a priori (nor its normal velocity V_Γ). Moreover, the interface position varies with time and this has major consequences on the adaptive strategy. The continuity of the temperature is natural in a finite element implementation but the heat flux equilibrium condition on Γ is not so easily enforced. One way to do so is to introduce the enthalpy formulation as described in the next section. A modification of the enthalpy formulation related to phase-field theory will also be introduced.

3. Enthalpy and semi-phase-field formulations

It is convenient to first recall the enthalpy formulation of the Stefan problem. The reader is referred to [3,5,11] for a complete discussion. One has to solve

$$\frac{\partial H}{\partial t} - \nabla \cdot (\boldsymbol{K} \nabla T) = f, \tag{2}$$

where $\boldsymbol{K} = \boldsymbol{K}_i$, $f = f_i$ in Ω_i and H is the enthalpy illustrated in Fig. 1 and defined by

$$H = \begin{cases} H_{\mathrm{s}} = \rho_{\mathrm{s}} c_{\mathrm{s}} T & \text{if } T < T_{\mathrm{f}}, \\ H_{\mathrm{l}} = \rho_{\mathrm{l}} L + \rho_{\mathrm{s}} c_{\mathrm{s}} T_{\mathrm{f}} + \rho_{\mathrm{l}} c_{\mathrm{l}} (T - T_{\mathrm{f}}) & \text{if } T > T_{\mathrm{f}}. \end{cases}$$

It can be shown that problem (2) is equivalent to the Stefan problem (1) and that the interface condition is automatically satisfied in the distributional sense, i.e.

$$\frac{\partial H}{\partial t} = \begin{cases} \rho_{\mathrm{s}} c_{\mathrm{s}} \frac{\partial T}{\partial t} & \text{in } \Omega_{\mathrm{s}}, \\ \rho_{\mathrm{l}} c_{\mathrm{s}} \frac{\partial T}{\partial t} & \text{in } \Omega_{\mathrm{l}}, \\ \rho_{\mathrm{l}} L V_\Gamma \boldsymbol{\delta}_\Gamma & \text{on } \Gamma. \end{cases}$$

The Dirac delta distribution $\boldsymbol{\delta}_\Gamma$ comes from the discontinuity of H as a function of T (see Fig. 1). On the other hand, phase-field formulation requires the introduction of the phase-field function ϕ defined as

$$\phi = \begin{cases} 0 & \text{in } \Omega_{\mathrm{s}}, \\ 1 & \text{in } \Omega_{\mathrm{l}}. \end{cases}$$

As illustrated in Fig. 2 the following decomposition is introduced:

$$H = H_1 + \rho_{\mathrm{l}} L \phi,$$

where H_1 is now a continuous function:

$$H_1 = \begin{cases} \rho_{\mathrm{s}} c_{\mathrm{s}} T & \text{in } \Omega_{\mathrm{s}}, \\ \rho_{\mathrm{s}} c_{\mathrm{s}} T_{\mathrm{f}} + \rho_{\mathrm{l}} c_{\mathrm{l}} (T - T_{\mathrm{f}}) & \text{in } \Omega_{\mathrm{l}}, \end{cases}$$

so that

$$\frac{\partial H_1}{\partial t} = \begin{cases} \rho_{\mathrm{s}} c_{\mathrm{s}} \frac{\partial T}{\partial t} & \text{in } \Omega_{\mathrm{s}}, \\ \rho_{\mathrm{l}} c_{\mathrm{l}} \frac{\partial T}{\partial t} & \text{in } \Omega_{\mathrm{l}}. \end{cases}$$

The Dirac delta function $\rho_{\mathrm{l}} L V_\Gamma \boldsymbol{\delta}_\Gamma$ now comes from the time derivative of the term $\rho_{\mathrm{l}} L \phi$. Replacing the last equation in system (2), a new formulation is obtained which is also equivalent to the classical Stefan problem. Eq. (2) now takes the following form:

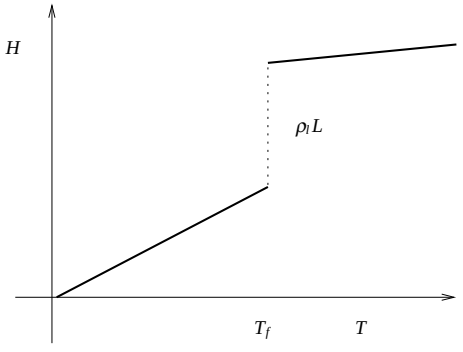

Fig. 1. Enthalpy–temperature relation.

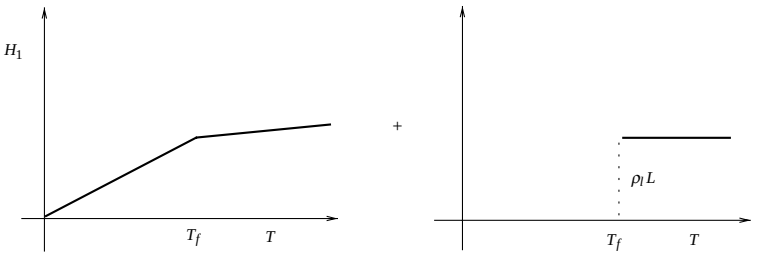

Fig. 2. Relation $H = H_1 + \rho_1 L\phi$.

$$\alpha(\phi)\frac{\partial T}{\partial t} + \rho L\frac{\partial \phi}{\partial t} - \nabla\cdot(\boldsymbol{K}(\phi)\nabla T) = f(\phi),$$

where

$$\begin{cases} \alpha(\phi) = \rho_s c_s + \phi(\rho_1 c_1 - \rho_s c_s), \\ \boldsymbol{K}(\phi) = \boldsymbol{K}_s + \phi(\boldsymbol{K}_1 - \boldsymbol{K}_s), \\ f(\phi) = f_s + \phi(f_1 - f_s). \end{cases}$$

The function ϕ has now to be computed. In phase-field theory (see [4,6,7,9]), an ordinary differential equation is introduced for the computation of ϕ. In this model it is preferable to use an algebraic equation but this simplification is valid only for the classical Stefan problem. For this reason this formulation is referred to as a semi-phase-field model. The algebraic equation takes the form

$$\phi = F(T) = \begin{cases} 0 & \text{if } T < T_f, \\ 1 & \text{if } T > T_f, \end{cases}$$

and the Stefan problem becomes equivalent to the following system:

$$\begin{cases} \alpha(\phi)\dfrac{\partial T}{\partial t} + \rho L\dfrac{\partial \phi}{\partial t} - \nabla\cdot(\boldsymbol{K}(\phi)\nabla T) = f(\phi), \\ \phi = F(T). \end{cases} \tag{3}$$

Problem (3) is equivalent to the Stefan problem (1) and can be easily extended to the case where ρ_i, c_i and $\boldsymbol{K}_i$ are functions of the temperature.

In applications, phase change is not always instantaneous and may occur in a small temperature range $[T_f - \epsilon, T_f + \epsilon]$. The relation for $F(T)$ can thus be replaced by a regularized one ($F_\epsilon(T)$) and it can be done in a number of more or less efficient ways. The idea is to connect the constant value 0 (for $T < T_f - \epsilon$) and the constant value 1 (for $T > T_f + \epsilon$) by a cubic Hermite polynomial

$$\phi = F_\epsilon(T) = \begin{cases} 0 & \text{if } T < T_f - \epsilon, \\ \text{cubic Hermite polynomial} & \text{if } T_f - \epsilon \leqslant T \leqslant T_f + \epsilon, \\ 1 & \text{if } T > T_f + \epsilon. \end{cases}$$

The resulting curve is differentiable as long as $\epsilon \neq 0$. The curve gets however stiffer as ϵ decreases. The functions α, $\boldsymbol{K}$, and f are then automatically regularized in a similar way since they depend on ϕ.

The regularized semi-phase-field equations are then given by

$$\begin{cases} \alpha(\phi)\dfrac{\partial T}{\partial t} + \rho L\dfrac{\partial \phi}{\partial t} - \nabla\cdot(\boldsymbol{K}(\phi)\nabla T) = f(\phi), \\ \phi = F_\epsilon(T). \end{cases} \tag{4}$$

3.1. Weak formulation and finite element discretization

The variational formulation corresponding to system (4) is straigthforward. To simplify the presentation, homogeneous boundary conditions are supposed for the temperature T but the general case follows the same lines. Multiplying the first equation by a test function v_T and the second by a (possibly discontinuous) test function v_ϕ, the variational formulation can be written as

$$\begin{cases} \int_\Omega \left(\alpha(\phi) \dfrac{\partial T}{\partial t} v_T + \rho_l L \dfrac{\partial \phi}{\partial t} v_T + (\boldsymbol{K}(\phi)\nabla T) \cdot \nabla v_T \right) \mathrm{d}\Omega = \int_\Omega f(\phi) v_T \, \mathrm{d}\Omega, \\ \int_\Omega (\phi - F_\epsilon(T)) v_\phi \, \mathrm{d}\Omega = 0. \end{cases}$$

Starting from the solution $T^{(n)}$ and $\phi^{(n)} = F_\epsilon(T^{(n)})$ at time $t^{(n)}$, a fully implicit Euler scheme is used for the time derivative discretization which gives

$$\frac{\partial T}{\partial t}(t^{(n+1)}) \simeq \frac{T^{(n+1)} - T^{(n)}}{\Delta t} \quad \text{and} \quad \frac{\partial \phi}{\partial t}(t^{(n+1)}) \simeq \frac{\phi^{(n+1)} - \phi^{(n)}}{\Delta t}.$$

The variational formulation becomes

$$\begin{cases} \int_\Omega \alpha(\phi^{(n+1)}) \left(\dfrac{T^{(n+1)} - T^{(n)}}{\Delta t} \right) v_T \, \mathrm{d}\Omega + \int_\Omega \rho_l L \left(\dfrac{\phi^{(n+1)} - \phi^{(n)}}{\Delta t} \right) v_T \, \mathrm{d}\Omega \\ \quad + \int_\Omega \boldsymbol{K}(\phi^{(n+1)}) \nabla T^{(n+1)} \cdot \nabla v_T \, \mathrm{d}\Omega = \int_\Omega f(\phi^{(n+1)}) v_T \, \mathrm{d}\Omega, \\ \int_\Omega \left(\phi^{(n+1)} - F_\epsilon(T^{(n+1)}) \right) v_\phi \, \mathrm{d}\Omega = 0. \end{cases} \tag{5}$$

This non-linear system is solved at each time step with Newton's method for example. The parameter ϵ has a smoothing effect but the problem can still be very stiff for small values of ϵ. Discontinuous approximation of ϕ may be considered such as piecewise constant or linear polynomials. This seems a natural thing to do when considering the discontinuous nature of ϕ. This was done in [5] where in absence of mesh adaptation, it was shown that discontinuous discretizations of ϕ provide better results. However, in this paper only continuous approximations are considered since mesh adaptation allows very accurate computation of the interface. Consequently, a quadratic discretization of the temperature T and a linear approximation of ϕ will be used in all numerical simulations.

4. Adaptive strategy

Many adaptive strategies have been developed in the last few years, in particular for phase change problems. In [8,9], a one-dimensional adaptive strategy was developed and many convincing numerical examples were presented. At each time step, the non-linear enthalpy equation is solved using a semi-implicit moving mesh discretization. In [11] an adaptive mesh refinement strategy is presented where three local parameters are used to equidistribute the interpolation error for the temperature. Two-dimensional isotropic meshes are obtained with a high concentration of elements near the interface. In [3], adapted grids are obtained from a mapping of the physical domain to the computational domain which is designed to concentrate the mesh around the interface. In both these works, isotropic meshes are obtained.

In this paper, attention will be given to the idea of hierarchical error estimator introduced in [1,2]. The major advantage is that the hierarchical method provides enough directional information to drive an anisotropic mesh adaptation procedure.

4.1. Hierarchical error estimator

The hierarchical method is based on a simple idea: given an approximation of order k say, a new approximation of order $k+1$ could be used to assess the accuracy of the solution. In the elliptic case, the continuous problem consists in finding $u \in V$ such that

$$a(u,w) = l(w) \quad \forall w \in V, \tag{6}$$

where a and l are, respectively, continuous bilinear and linear forms on an appropriate functional space V. If now $V_{h,k} \subset V$ denotes the discrete space of piecewise continuous polynomials of degree k, the approximate solution is obtained by finding $u_{h,k} \in V_{h,k}$ such that

$$a(u_{h,k}, w_{h,k}) = l(w_{h,k}) \quad \forall w_{h,k} \in V_{h,k}.$$

It is easily shown that the resulting error $e_k = u - u_{h,k}$ is the solution of

$$a(e_k, w) = r(w) \quad \forall w \in V,$$

where $r(w) = l(w) - a(u_{h,k}, w)$ is the residual. An approximation of this error can be obtained by considering the space $V_{h,k+1}$ of piecewise continuous polynomials of degree $k+1$ and by solving

$$a(e_{h,k+1}, w_{h,k+1}) = r(w_{h,k+1}) \quad \forall w_{h,k+1} \in V_{h,k+1}.$$

This would imply computing a full problem in the space $V_{h,k+1}$, which would obviously be prohibitive. The idea is then to use a hierarchical finite element basis of the space $V_{h,k+1}$:

$$V_{h,k+1} = V_{h,k} + C_{h,k+1},$$

so that $V_{h,k+1}$ is the direct sum of $V_{h,k}$ (polynomials of degree k) and a correction space $C_{h,k+1}$ consisting of polynomials of degree $k+1$. The error can be approximated by solving the following problem:

$$a(\hat{e}_{h,k+1}, c_{h,k+1}) = r(c_{h,k+1}) \quad \forall c_{h,k+1} \in C_{h,k+1}. \tag{7}$$

This means solving a new global problem whose dimension is that of $C_{h,k+1}$ which is much smaller than $V_{h,k+1}$. For elliptic partial differential equations this is well conditioned problem (the condition number does not depend on the mesh size) which can be solved in a few iterations by any simple iterative method such as the successive over-relaxation method or the conjugate gradient method. This approach was successfully used in Ndikumagenge [10].

It is however preferable to avoid completely having to solve any global problem. Moreover, in practice problems are not always of elliptic type and the above strategy become cumbersome. The idea is thus to compute the error in $C_{h,k+1}$ in a different way. To achieve this goal, problem (7) is rewritten as

$$a(u_{h,k} + \hat{e}_{h,k+1}, c_{h,k+1}) = l(c_{h,k+1}) \quad \forall c_{h,k+1} \in C_{h,k+1}, \tag{8}$$

so that the error can be seen as a degree $k+1$ hierarchical complement to the degree k solution $u_{h,k}$. Consequently, if by one way or another, a hierarchical complement to $u_{h,k}$ can be constructed consistent with problem (6), then it will be an approximation of the error in problem (7).

This idea was explored in [14] where they have made an experimental evaluation of some estimation procedures. In practice, an approximation of the hierarchical method was used, based on a smooth reinterpolation of the computed solution $u_{h,k}$ that shall be described in the following section.

4.2. Approximation of the hierarchical error estimator

In this section a heuristic way of approximating the hierarchical estimator is described. The practical advantage of this method is that it can be used independently of the problem (even without knowing the

problem). Only the solution $u_{h,k}$ and its corresponding mesh have to be provided. The technique essentially relies on the assumption that a reasonable estimate of the error can be obtained from a suitable reinterpolation of the numerical solution $u_{h,k}$. One example of such a procedure will now be presented.

Starting from a standard C^0 finite element solution $u_{h,k}$ of degree k, an approximation of the first and second-order derivatives at the vertices of the triangulation is needed. Since $u_{h,k}$ is not differentiable, a way to do that is by fitting a local quadratic interpolation on every vertex $\boldsymbol{P} = (x_P, y_P)$ of the mesh. One then has to define a patch of elements adjacent to the vertex $\boldsymbol{P}$ (see Fig. 3). This patch is also called a shell and denoted $\mathscr{S}$. It is also possible (and in some cases necessary) to include elements not directly connected to the vertex. Over this shell, the solution is approximated by a quadratic (truncated) Taylor series

$$u^{app}(x,y) = u_{h,k}(x_P,y_P) + u_x^{app}(x_P,y_P)(x-x_P) + u_y^{app}(x_P,y_P)(y-y_P) + u_{xx}^{app}(x_P,y_P)\frac{(x-x_P)^2}{2} + u_{xy}^{app}(x_P,y_P)(x-x_P)(y-y_P) + u_{yy}^{app}(x_P,y_P)\frac{(y-y_P)^2}{2},$$

where only $u_{h,k}(x_P, y_P)$ is known. Let us suppose that the patch of elements adjacent to vertex (x_P, y_P) contains N vertices $\boldsymbol{P}_i = (x_i, y_i)$, the idea is then to determine the best values of first- and second-order derivatives in a least square sense, i.e. values minimizing the Euclidian norm of the vector

$$\begin{bmatrix} u^{app}(x_1,y_1) - u_{h,k}(x_1,y_1) \\ u^{app}(x_2,y_2) - u_{h,k}(x_2,y_2) \\ u^{app}(x_3,y_3) - u_{h,k}(x_3,y_3) \\ \vdots \\ u^{app}(x_N,y_N) - u_{h,k}(x_N,y_N) \end{bmatrix}.$$

This minimization problem can be written in matrix form as

$$\min_{\boldsymbol{y}} \|B\boldsymbol{y} - \boldsymbol{b}\|_2 \tag{9}$$

where

$$\boldsymbol{y} = \begin{bmatrix} u_x^{app}(x_P,y_P) \\ u_y^{app}(x_P,y_P) \\ u_{xx}^{app}(x_P,y_P) \\ u_{xy}^{app}(x_P,y_P) \\ u_{yy}^{app}(x_P,y_P) \end{bmatrix}, \quad \boldsymbol{b} = \begin{bmatrix} u_{h,k}(x_1,y_1) - u_{h,k}(x_P,y_P) \\ u_{h,k}(x_2,y_2) - u_{h,k}(x_P,y_P) \\ u_{h,k}(x_3,y_3) - u_{h,k}(x_P,y_P) \\ \vdots \\ u_{h,k}(x_N,y_N) - u_{h,k}(x_P,y_P) \end{bmatrix}$$

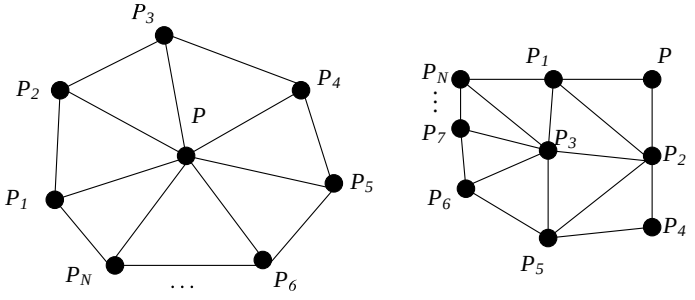

Fig. 3. Vertices adjacent to P.

and B is the $N \times 5$ matrix

$$B = \begin{bmatrix} (x_1 - x_P) & (y_1 - y_P) & \frac{1}{2}(x_1 - x_P)^2 & (x_1 - x_P)(y_1 - y_P) & \frac{1}{2}(y_1 - y_P)^2 \\ (x_2 - x_P) & (y_2 - y_P) & \frac{1}{2}(x_2 - x_P)^2 & (x_2 - x_P)(y_2 - y_P) & \frac{1}{2}(y_2 - y_P)^2 \\ (x_3 - x_P) & (y_3 - y_P) & \frac{1}{2}(x_3 - x_P)^2 & (x_3 - x_P)(y_3 - y_P) & \frac{1}{2}(y_3 - y_P)^2 \\ \vdots & \vdots & \vdots & \vdots & \vdots \\ (x_N - x_P) & (y_N - y_P) & \frac{1}{2}(x_N - x_P)^2 & (x_N - x_P)(y_N - y_P) & \frac{1}{2}(y_N - y_P)^2 \end{bmatrix}.$$

Once this system has been solved, the solution $u_{h,k}$ and approximations of all its first and second-order derivatives are known at the triangulation vertices. It is then possible to build a Hermite approximation of degree 5 in each element which is seemingly a better approximation to the exact solution u than $u_{h,k}$. This Hermite polynomial will be used to construct the hierarchical complement to $u_{h,k}$ in $V_{h,k+1}$. The idea will be illustrated in the linear case $k = 1$. The situation is slightly more complicated for higher degree polynomials but it follows the same lines (see [10]).

Let $u_{h,1}$ be a piecewise linear solution. In a hierarchical quadratic basis, the exact solution u can be interpolated on each triangular element as

$$u(\boldsymbol{x}) \simeq \sum_{i=1}^{3} \alpha_i(u)\psi_{1,i}(\boldsymbol{y}) + \sum_{i=1}^{3} \beta_i(u)\psi_{2,i}(\boldsymbol{x}),$$

where $\psi_{1,i}(\boldsymbol{x})$ are linear basis functions associated to the vertices of the element while the basis functions $\psi_{2,i}(\boldsymbol{x})$ are polynomials of degree 2 associated to the triangle mid-edges. The degrees of freedom α_i and β_i are functions of u. In a standard quadratic basis, the α's are nodal values of f ($\alpha_i = u(\boldsymbol{P}_i)$, $i = 1, 2, 3, \ldots, 6$) but in a hierarchical basis, it is easily shown that the degrees of freedom are given by

$$\alpha_i(u) = u(\boldsymbol{P}_i) \quad \text{and} \quad \beta_i(u) = u(\boldsymbol{M}_{ij}) - \frac{u(\boldsymbol{P}_i) + u(\boldsymbol{P}_j)}{2}, \qquad i = 1, 2, 3, \tag{10}$$

where $(\boldsymbol{M}_{ij})$ is the mid-side node of the edge between vertices $\boldsymbol{P}_i$ and $\boldsymbol{P}_j$. From Section 4.2, the following expression has to be evaluated to obtain an approximation of the error:

$$\hat{e}_{h,2} \simeq \sum_{i=1}^{3} \beta_i(u)\psi_{2,i}(\boldsymbol{x})$$

and these β_i's are approximated using the second part of Eq. (10) and replacing u by the degree 5 Hermite polynomial previously described. The procedure is similar with a quadratic approximation $k = 2$ and the error is then of degree 3 as described in [10].

4.3. Anisotropic mesh adaptation

The objective of mesh adaptation is, starting from a solution on an initial mesh, to provide a new mesh where a prescribed absolute error e_d is reached everywhere in the domain. The mesh adaptation procedure is based on a number of local operations on the initial mesh:

- edge refinement;
- edge swapping;
- vertex suppression;
- vertex displacement.

This sequence is repeated 8–10 times until the mesh stabilizes. The decision whether a given local operation has to be performed is based on the definition of the error on an element K and on its gradient, respectively, defined by

$$\|E\|_K = \left(\int_K |\hat{e}_{h,k+1}|^2 \, \mathrm{d}K \right)^{1/2} \quad \text{and} \quad \|\nabla E\|_K = \left(\int_K |\nabla \hat{e}_{h,k+1}|^2 \, \mathrm{d}K \right)^{1/2}.$$

The local operations are used with two objectives: control the error level on each element so that the absolute error takes the value e_d everywhere. On each element K, this implies that

$$\|E\|_K \simeq \left(\int_K |e_d|^2 \, \mathrm{d}K \right)^{1/2} = e_d (\mathrm{area}(K))^{1/2}.$$

The second objective is to achieve equidistribution of this error by minimizing the error gradient. If the error gradient vanishes, than the error is everywhere constant and takes the value e_d. Edge refinement and vertex suppression are used in order to control the error level while vertex displacement and edge swapping are used to minimize its gradient. As shall be seen, this procedure is enough to provide strongly anisotropic meshes and very accurate solutions.

In each local operation, a shell S is constructed consisting of adjacent elements. For the operations on the edges, the shell usually consists of the two elements adjacent to that edge while for operations acting on the vertices, the shell is the patch of surrounding elements. In some pathological cases (not discussed here), more attention has to be given to the construction of the shell.

The algorithm consists in sweeping the vertices and edges repeatedly and determine if a given local operation is needed:

- Edge refinement (see Fig. 4).

  An edge will be cut in halves if

$$\sum_{K \in S} \int_K |\hat{e}_{h,k+1}|^2 \, \mathrm{d}K > \sum_{K \in S} \int_K |e_d|^2 \, \mathrm{d}K,$$

  thus eliminating the two triangles of shell S and creating a new shell S' consisting of four new triangles.
- Vertex suppression (see Fig. 5).

  If

$$\sum_{K \in S} \int_K |\hat{e}_{h,k+1}|^2 \, \mathrm{d}K < \sum_{K \in S} \int_K |e_d|^2 \, \mathrm{d}K,$$

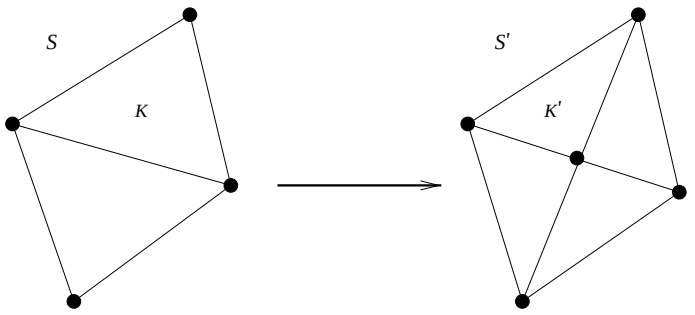

Fig. 4. Edge refinement.

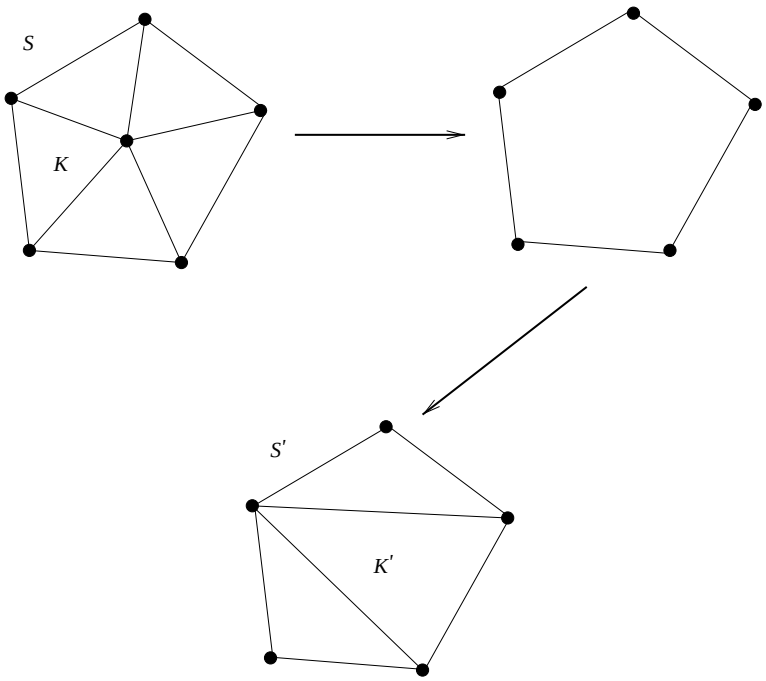

Fig. 5. Vertex suppression.

then the vertex will be removed at the additional condition that

$$\sum_{K' \in S'} \int_{K'} |\hat{e}_{h,k+1}|^2 \, \mathrm{d}K' < \sum_{K' \in S'} \int_{K'} |e_d|^2 \, \mathrm{d}K',$$

where K' are the new elements obtained by removing the vertex.

- Edge swapping (see Fig. 6).

  The edge between two triangles will be swapped if

$$\sum_{K \in S} \int_{K} |\nabla \hat{e}_{h,k+1}|^2 \, \mathrm{d}K > \sum_{K' \in S'} \int_{K'} |\nabla \hat{e}_{h,k+1}|^2 \, \mathrm{d}K'.$$

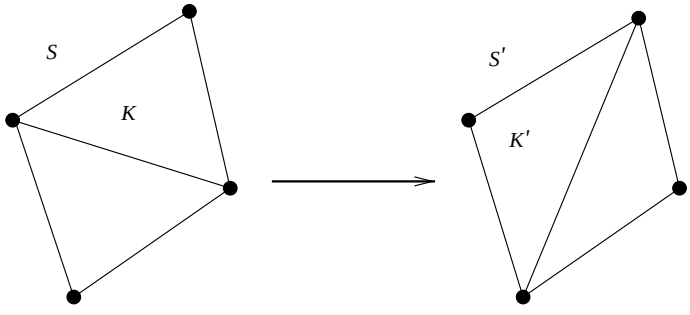

Fig. 6. Edge swapping.

- Vertex displacement (see Fig. 7).

  A vertex will be moved inside the shell in such a way that

$$\sum_{K\in S}\int_K |\nabla \hat{e}_{h,k+1}|^2\,\mathrm{d}K > \sum_{K'\in S'}\int_{K'} |\nabla \hat{e}_{h,k+1}|^2\,\mathrm{d}K'.$$

Each time a new vertex is created (edge refinement) or moved, the solution $u_{h,k}$ and its first and second-order derivatives must be reinterpolated at the vertex location in order to pursue the adaptation process. Suppose that this new vertex is located in some element K. The value of $u_{h,k}$ is computed using the fifth-order polynomial constructed in Section 4.2. Second-order derivatives are known at the vertices of element K and consequently a linear interpolation can be used to determine second-order derivatives at the new vertex location. Finally, a linear interpolation could also be used for first-order derivatives but there exists a better solution. Indeed, first-order derivatives are known at vertices together with second-order derivatives. Consequently, a third-order Hermite interpolation can be used to interpolate first-order derivatives.

The procedure described in this section can be modified to take more than one scalar solution into account when adapting the mesh. For systems of equations and time-dependent problems, this is necessary. The idea is very simple and will be used later on. Once the pertinent adaptation variables have been chosen, an error level e_d is established for each variable, possibly different from one variable to the other. This choice is delicate since the adaptation variables may have values of totally different scales. Then, the local operations are performed in order to determine the mesh best suited for all variables. For example, an edge will be cut if the estimated error on one of the variable is too large. A vertex will be removed if the corresponding criterion is satisfied for all variables and so on. As shall be seen, this procedure can be used for time-dependent problems where the mesh can be adapted to the solution at different times.

4.4. Adaptive strategy for time-dependent problems

The overall adaptive strategy is the following:

1. Starting from a solution $(T^{(n)}, \phi^{(n)})$ and a mesh $\mathscr{M}^{(n)}$ at time $t^{(n)}$.
2. Solve system (5) on mesh $\mathscr{M}^{(n)}$ to obtain a first approximation $(\tilde{T}^{(n+1)}, \tilde{\phi}^{(n+1)})$ of the solution at time $t^{(n+1)}$.
3. Adapt the mesh on the new solution $(\tilde{T}^{(n+1)}, \tilde{\phi}^{(n+1)})$ and $(T^{(n)}, \phi^{(n)})$ to obtain $\mathscr{M}^{(n+1)}$.
4. Reinterpolate $(T^{(n)}, \phi^{(n)})$ on $\mathscr{M}^{(n+1)}$.
5. Solve system (5) on mesh $\mathscr{M}^{(n+1)}$ for $(T^{(n+1)}, \phi^{(n+1)})$.

It is worth mentioning a few words about this strategy. The mesh has to be adapted at each time step in order to preserve the accuracy of the solution. A crucial step is the reinterpolation of $(T^{(n)}, \phi^{(n)})$ on the mesh $\mathscr{M}^{(n+1)}$. If care is not taken and if the new mesh is not well adapted to the solution $(T^{(n)}, \phi^{(n)})$, this reinterpolation can give very poor results. This is why in step 3, the mesh is adapted on the four variables $(\tilde{T}^{(n+1)}, \tilde{\phi}^{(n+1)})$ and on $(T^{(n)}, \phi^{(n)})$ to avoid inaccurate reinterpolation of the solution at time $t^{(n)}$ on the mesh $\mathscr{M}^{(n+1)}$. The resulting mesh is thus adapted to the actual and preceeding solutions.

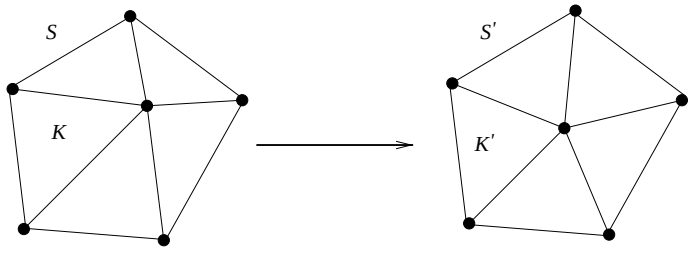

Fig. 7. Vertex displacement.

It is also possible to modify the above strategy and adapt the mesh only on $\tilde{\phi}^{(n+1)}$ (and $\phi^{(n)}$). The freezing front is then well captured but the temperature is slightly less accurate. However, the number of elements is greatly reduced since the mesh is refined only in the vicinity of the interface. In the numerical results, examples will be shown where both strategies were employed.

5. Numerical results

In this section, four different problems assessing the reliability and accuracy of the proposed numerical method and adaptive strategy will be presented. Starting with two problems having analytical solutions, comparisons between analytical and numerival solutions will be performed. The last two problems are classical benchmarks for phase change computations.

5.1. Stefan problem with analytical solution

The first test case is a one-dimensional example for which there exists an analytical solution (see [13]). Although the problem is one-dimensional, the computation will be performed in two dimensions.

The computational domain is the rectangle $[0,2]\times[0,1]$. The temperature is maintained fixed on the side $x=0$ ($T(0,y,t)=T_1$) while homogeneous Neumann conditions are imposed on all the other sides. The thermal conductivities tensors are isotropic and take the form $\boldsymbol{K}_s = K_s\boldsymbol{I}$ and $\boldsymbol{K}_l = K_l\boldsymbol{I}$, where I is the unit tensor. The x-position of the solid–liquid interface is noted $X_f(t)$ and is given by (see [13])

$$X_f(t) = 2\lambda\sqrt{\kappa_s t}, \tag{11}$$

while the analytical temperature is given by

$$T = \begin{cases} T_l + \dfrac{T_f - T_l}{\operatorname{erf}(\lambda)}\operatorname{erf}\left(\dfrac{x}{2\sqrt{\kappa_s t}}\right) & \text{if} \quad x < X_f(t), \\ T_0 - (T_0 - T_f)\dfrac{\operatorname{erfc}\left(\dfrac{x}{2\sqrt{\kappa_s t}}\right)}{\operatorname{erfc}\left(\dfrac{\lambda\sqrt{\kappa_s}}{\sqrt{\kappa_l}}\right)} & \text{if} \quad x \geqslant X_f(t), \end{cases} \tag{12}$$

where

$$\operatorname{erf}(x) = \frac{2}{\sqrt{\pi}}\int_0^x \mathrm{e}^{-t^2}\,\mathrm{d}t, \quad \operatorname{erfc}(x) = 1 - \operatorname{erf}(x),$$

and $\kappa_s = K_s/\rho_s c_s$, $\kappa_l = K_l/\rho_l c_l$ and T_0 is the initial temperature. The value of the parameter λ is a solution of the following non-linear equation:

$$\frac{\mathrm{e}^{-\lambda^2}}{\operatorname{erf}(\lambda)} - \frac{(T_0 - T_f)\sqrt{\kappa_{sl}}}{(T_f - T_l)K_{sl}}\frac{\mathrm{e}^{-\lambda\kappa_{sl}}}{\operatorname{erfc}(\lambda\sqrt{\kappa_{sl}})} - \frac{\sqrt{\pi}\rho_l L\lambda\kappa_s}{K_s(T_f - T_l)} = 0, \tag{13}$$

where $\kappa_{sl} = \kappa_s/\kappa_l$ and $K_{sl} = K_s/K_l$. In the numerical simulations the following values have been used:

$$\begin{array}{ll} T_0 = 0\ ^\circ\mathrm{C}, & \rho_s = \rho_l = 1, \\ T_l = -45\ ^\circ\mathrm{C}, & c_s = c_l = 1, \\ T_f = -0.15\ ^\circ\mathrm{C}, & K_s = K_l = 1.08, \\ \lambda = 0.51531, & L = 70.26. \end{array} \tag{14}$$

With these values, the non-linear equation (13) was solved (by a secant method for example) and the value $\lambda = 0.51531$ was obtained. The initial temperature was set to 0 and since at that time there is no solid region, $X(0) = 0$.

Fig. 8 presents the initial mesh together with its time evolution. The one-dimensional nature of the solution is clearly seen. The elements are strongly elongated in the y-direction and concentrated in the vicinity of the front. On the walls, the elements are not as elongated as in the middle of the domain. No satisfactory explanation was found for this behaviour. This is probably due to the approximation of the hierarchical error estimator which is less accurate on the boundary since the construction of the shell for solving Eq. (9) is more delicate. The last picture in Fig. 8 shows the elongation of the elements in the region of the front and on the bottom wall of the domain at $t = 1.6$. Fig. 9 shows the numerical solution T and ϕ at time $t = 1$. The discontinuity of ϕ is very well captured, thanks to the high element concentration near the discontinuity. Finally, Fig. 10 shows a superposition of the numerical and analytical solutions at time $t = 1$ and $t = 2$. They are almost undistinguishable.

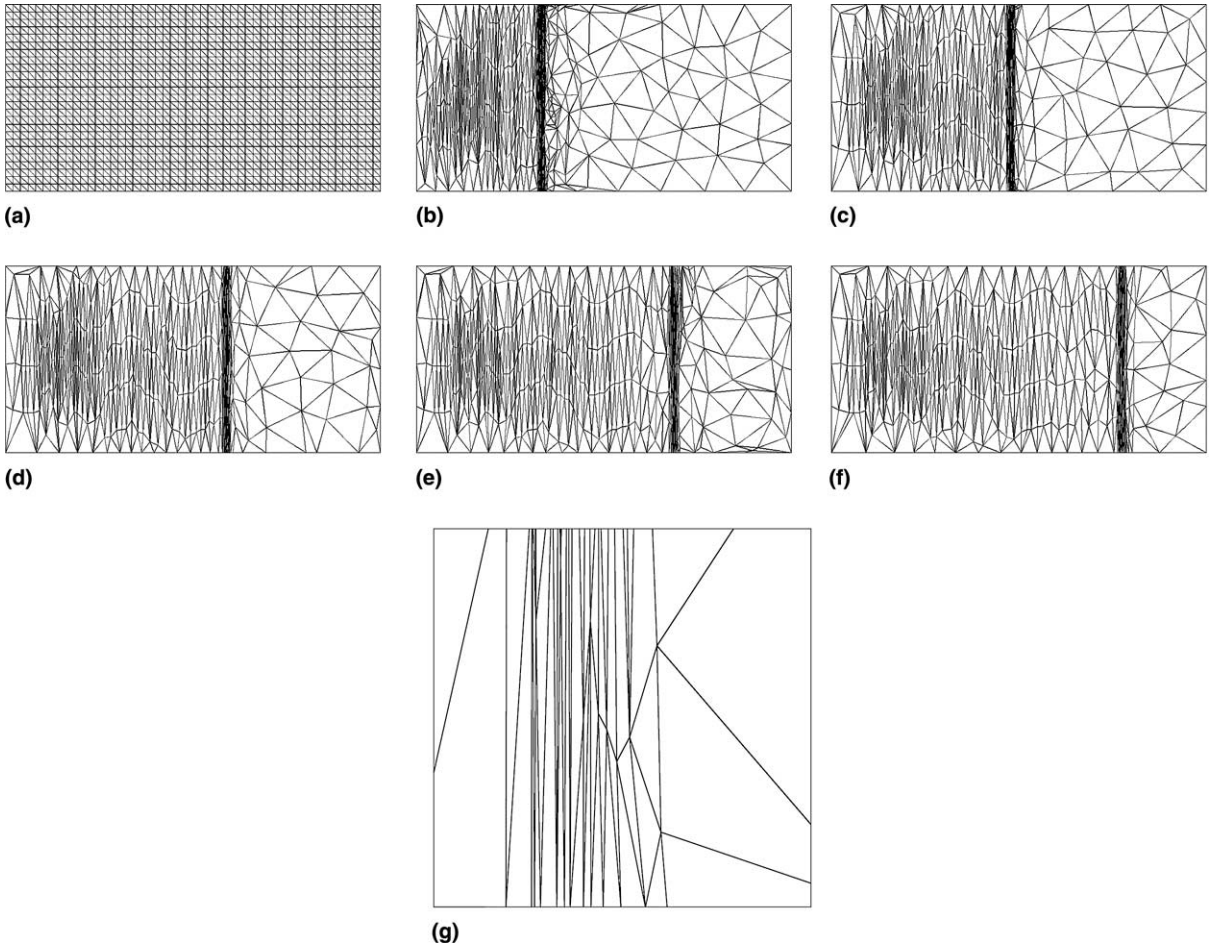

Fig. 8. Evolution of the front for the one-dimensional problem. (a) $t = 0$; (b) $t = 0.4$; (c) $t = 0.8$; (d) $t = 1.2$; (e) $t = 1.6$; (f) $t = 2$; (g) close up view near the wall.

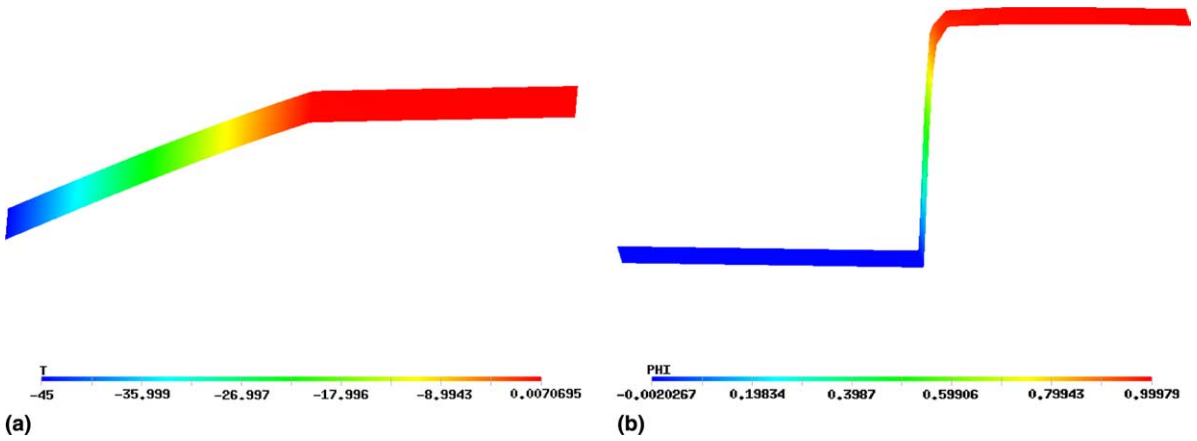

Fig. 9. Computed solutions for T and ϕ at $t = 1$. (a) T at $t = 1$; (b) ϕ at $t = 1$.

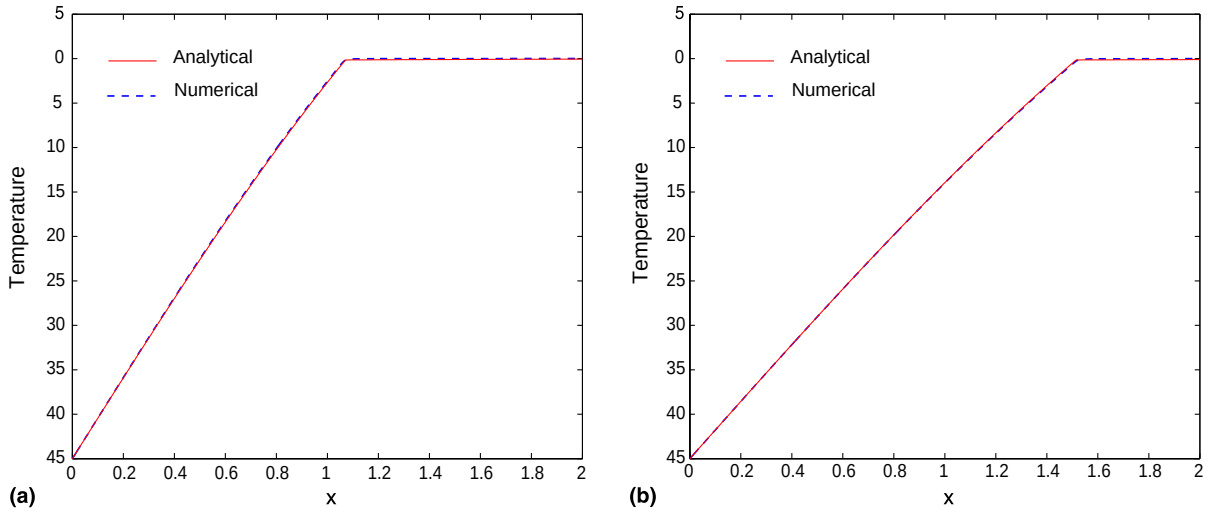

Fig. 10. Superposition of analytical and numerical temperature at $t = 1$ and $t = 2$. (a) $t = 1$; (b) $t = 2$.

5.2. Oscillating circle

In this problem, a circular freezing front interface oscillating in a square cavity is considered. This problem was also solved in [12]. For this specific problem, the form of the freezing front is fixed (a circle of radius 1/6) while its position varies with time.

The computational domain is the square $\Omega = [0.1, 0.7] \times [0.2, 0.8]$. The center of the circle is moving up and down along the axis $x = 1/3$ and is located at position $(1/3, \alpha(t))$ with $\alpha(t) = 0.5 + 0.1\sin(12.5t)$. The period of oscillation is thus $4\pi/25$. The main interest of this problem is that there exists an analytical solution for the temperature given by

$$T(x, y, t) = \begin{cases} 0.75(6r^2 - 1/6) & \text{if } r < 1/6, \\ (1.5 - \dot{\alpha}(t)\sin\phi)(r - 1/6) & \text{if } r \geqslant 1/6, \end{cases} \tag{15}$$

where $r = ((x - 1/3)^2 + (y - \alpha(t))^2)^{1/2}$, $\sin\phi = ((y - \alpha(t))/r)$ and $\dot{\alpha}(t) = (\mathrm{d}\alpha/\mathrm{d}t)(t)$. This function is a solution of the Stefan problem (1) if a proper source term f is provided. This can be done by inserting the solution (15) in the left-hand side of the first equation of system (1). The proper right-hand side f is easily obtained using Maple for instance.

Boundary conditions must also be provided. In this case, Dirichlet boundary conditions compatible with the analytical solution are given on all sides. The initial condition is also compatible with solution (15). The other parameters are given in the following table:

$$\begin{array}{ll} \rho_s = \rho_l = 1 & L = 1, \\ c_s = c_l = 1 & T_f = 0, \\ K_s = K_l = 1. & \end{array} \tag{16}$$

Fig. 11 shows the evolution of the mesh with time. The interface is clearly seen and is very close to the analytical position. Indeed, Fig. 12 shows the L^2 norm of the error on the temperature. In this problem, the target absolute value e_d on the temperature was fixed to 0.001. If this target value is attained, then one should have

$$\|E\|_{2,\Omega} \simeq e_d(\mathrm{area}(\Omega))^{1/2} = 6.0 \times 10^{-4},$$

which is very close to the values observed in Fig. 12.

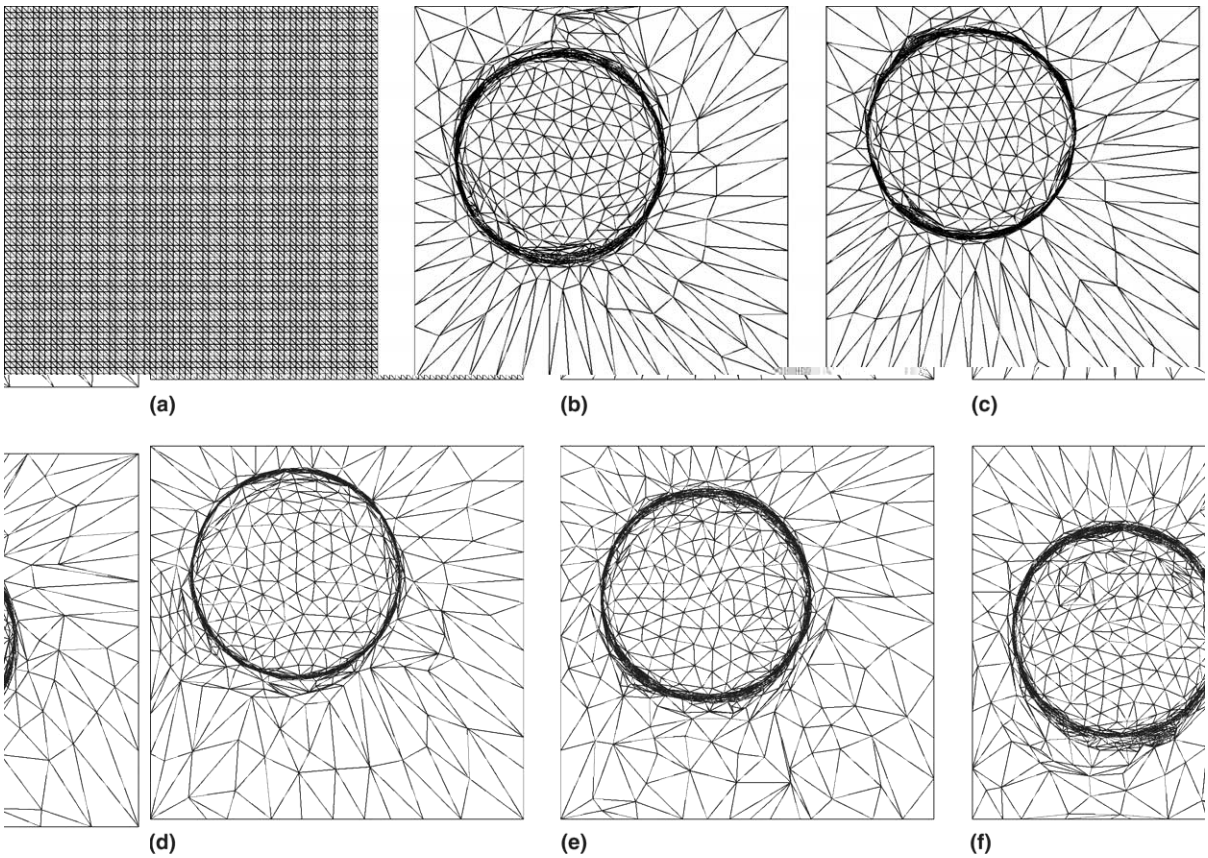

Fig. 11. Mesh evolution for the oscillating circle. (a) $t = 0$; (b) $t = 4\pi/250$; (c) $t = 8\pi/250$; (d) $t = 12\pi/250$; (e) $t = 16\pi/250$; (f) $t = 20\pi/250$.

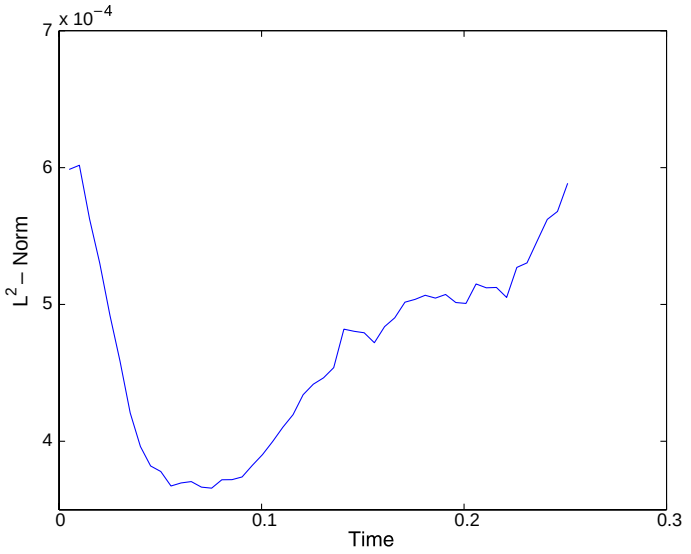

Fig. 12. L^2-norm of the error.

5.3. Oscillating source

This problem was also solved in [3] and [4]. The computational domain is the square $[-1,1]\times[-1,1]$. The initial temperature is given by $T(x,y,0)=y/10$. A Dirichlet boundary condition $T(x,y,t)=y/10$ is enforced on the left, right and top sides while a homogeneous Neumann condition is imposed on the last side ($y=-1$). The heat source f for this problem is given by

$$f(x,,y,t) = \cos\left(\frac{t}{5}\right)\max\left(0, 3.125 - 50\left(\left(x+\frac{1}{5}\right)^2 + \left(y+\frac{1}{2}\right)^2\right)\right) + \sin\left(\frac{t}{5}\right)\max\left(0, 3.125 - 50\left(\left(x+\frac{1}{5}\right)^2 + \left(y-\frac{1}{2}\right)^2\right)\right).$$

No exact solution is known for this problem. The interest of this problem is that the source term is time-oscillating thus provoking strong local changes in the interface position and form as illustrated in Fig. 13 where the mesh was adapted taking into account the variations of T and ϕ. As can be seen, the mesh is concentrated near the interface which evolves rapidly. The mesh also detects the influence of the source term which provokes two slightly concentrated spots in the mesh.

It is also possible to adapt the mesh only on the variable ϕ as illustrated in Fig. 14. The number of elements is greatly reduced since the mesh is almost uniform far from the interface. This gain in computational time introduces a small inaccuracy in the variable T but the interface position is still very well predicted. Fig. 15 presents two and three-dimensional views of the evolution of the interface ϕ with time. Very shasp transitions for ϕ can be observed. The numerical results presented in this paper are certainly comparable to those previously observed in the literature (see [3,4]).

Finally, the influence of the prescribed value of the absolute error e_d (see Section 4.3) on the number of elements was tested. This is illustrated in Fig. 16 where the time-evolution of the number of elements in the

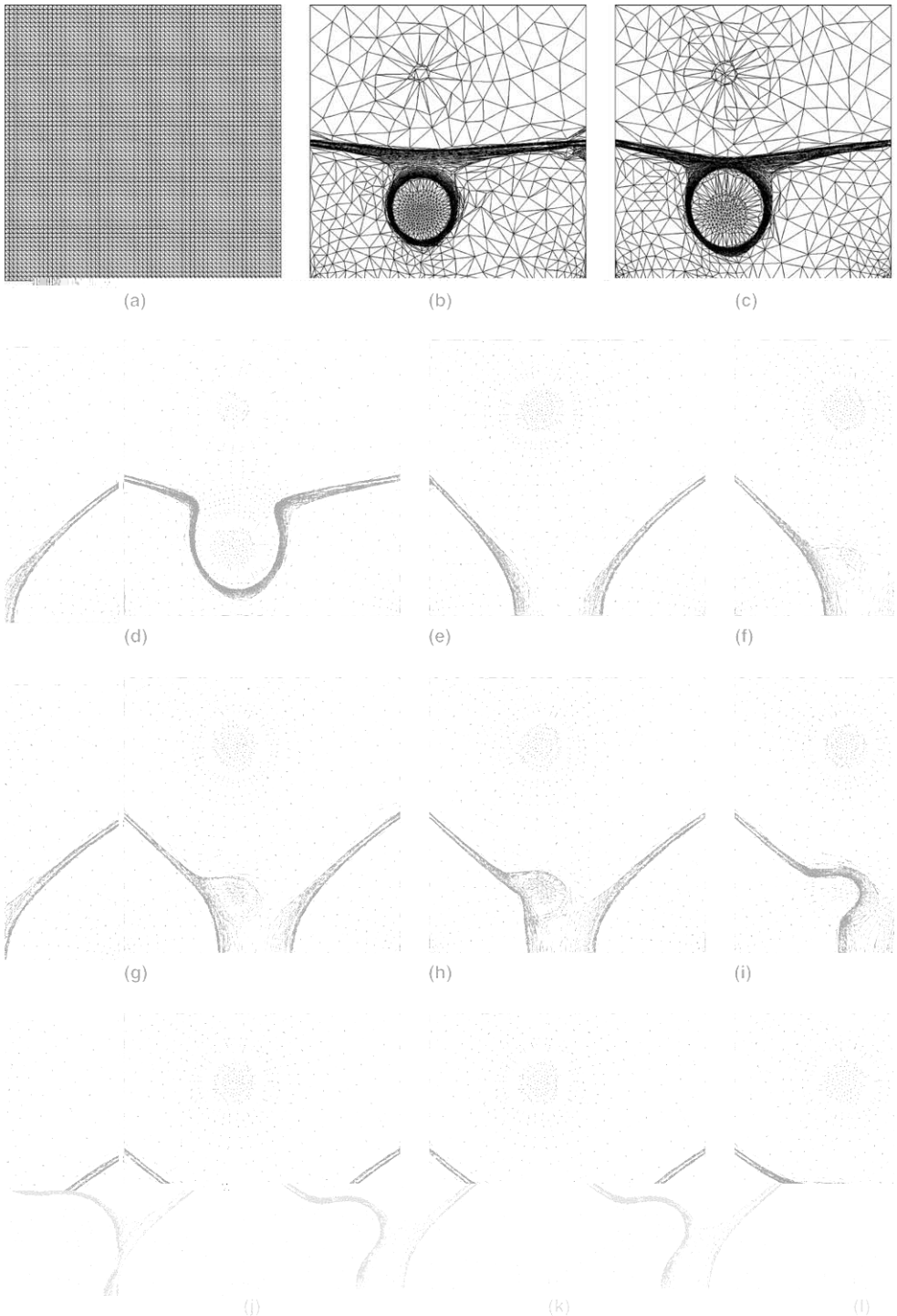

Fig. 13. Oscillating source: adaptation on T and ϕ. (a) $t = 0$; (b) $t = 1$; (c) $t = 1.5$; (d) $t = 2$; (e) $t = 8.5$; (f) $t = 9$; (g) $t = 9.5$; (h) $t = 10$; (i) $t = 10.5$; (j) $t = 11$; (k) $t = 11.5$; (l) $t = 12$.

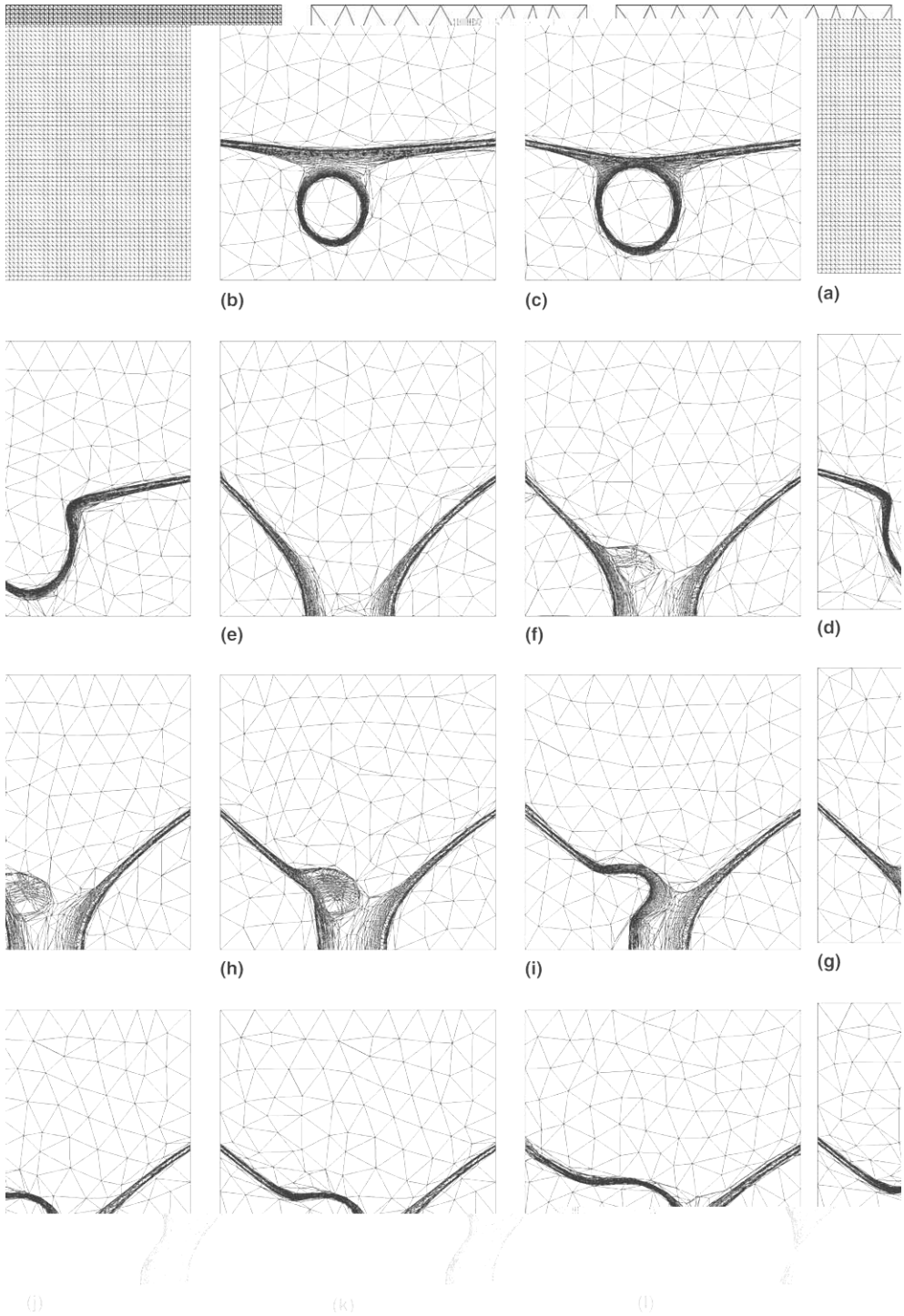

Fig. 14. Oscillating source: adaptation on ϕ only. (a) $t = 0$; (b) $t = 1$; (c) $t = 1.5$; (d) $t = 2$; (e) $t = 8.5$; (f) $t = 9$; (g) $t = 9.5$; (h) $t = 10$; (i) $t = 10.5$; (j) $t = 11$; (k) $t = 11.5$; (l) $t = 12$.

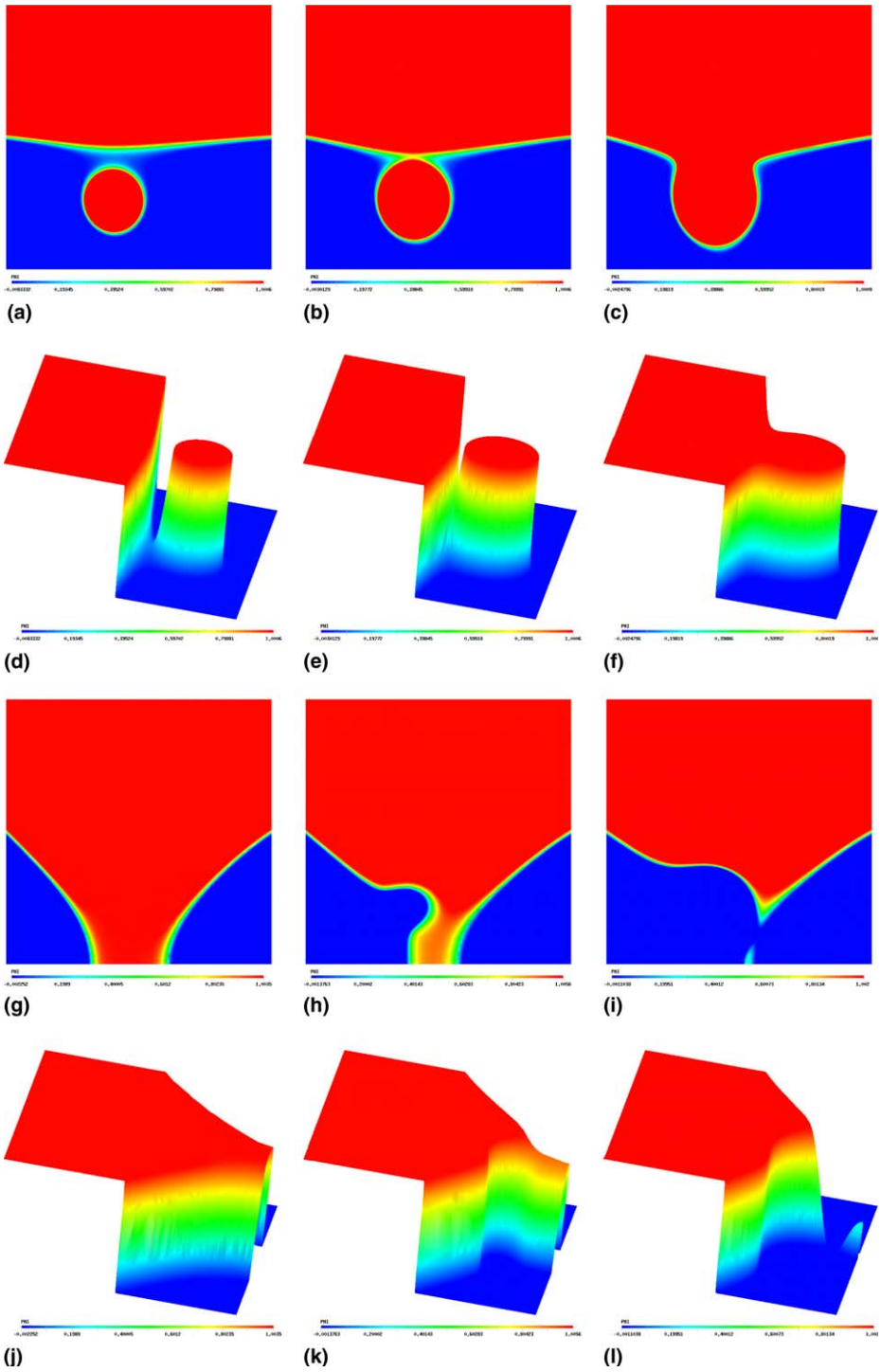

Fig. 15. Oscillating source: time-evolution of the interface ϕ. (a) $t = 1$; (b) $t = 1.5$; (c) $t = 2$; (d) $t = 1$; (e) $t = 1.5$; (f) $t = 2$; (g) $t = 8.5$; (h) $t = 10$; (i) $t = 12$; (j) $t = 8.5$; (k) $t = 10$; (l) $t = 12$.

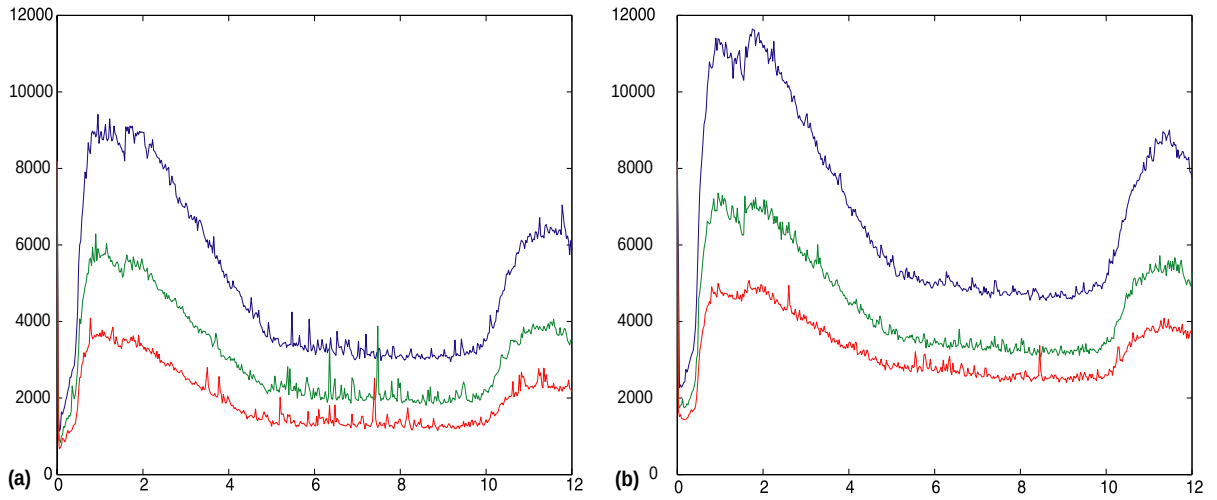

Fig. 16. Oscillating source: number of elements vs time for $e_d = 0.0025$, 0.0015 and 0.0009. (a) Adaptation on ϕ, (b) adaptation on T and ϕ.

meshes of Figs. 13 and 14 is illustrated. As expected, the smaller the value of e_d, the larger the number of elements. Moreover, adapting on ϕ only reduces by 20–25% the number of elements. The six curves have almost exactly the same form and the number of elements obviously follows the complexity of the interface form.

5.4. Formation of a cusp

In the last example, the freezing front takes the form of a cusp which gradually shrinks to nothing at time $t = 1$. This problem was also solved in [3] and [11]. The computational domain is the rectangle $[-2, 4] \times [0, 5]$. The initial temperature is given by

$$T_0(x,y) = \begin{cases} 0.25(r^2-1) & \text{for } r \leqslant 1,\ y \geqslant 2, \\ 0.25(x^2-1) & \text{for } |x| > 1,\ y < 1, \\ (r-1) & \text{for } r > 1,\ y \geqslant 2, \\ 5(|x|-1) & \text{for } |x| > 1,\ y < 1, \\ (|x|-1)(3-2\cos\pi(y-2)) & \text{for } |x| > 1,\ 1 \leqslant y < 2, \end{cases}$$

where $r = \sqrt{x^2+y^2}$. A time-dependent Dirichlet boundary condition

$$T = (1+t)T_0(x,y),$$

is enforced on the sides $x = -2$, $x = 4$ and $y = 5$ while a homogeneous Neumann condition is imposed on the last side. The boundary conditions are thus time dependent.

Fig. 17 shows once again the evolution of the meshes when adapting the mesh on both T and ϕ. The mesh is still well adapted to preserve the accuracy of the temperature solution The cusp gradually shrinks to nothing at time $t = 1$. The figure also clearly shows the presence of regions where the elements are concentrated due to the boundary conditions which are detected by the adaptation on the variable T. The adaptation on the variable ϕ only (see Fig. 18) was also tested. Here again, the number of elements is

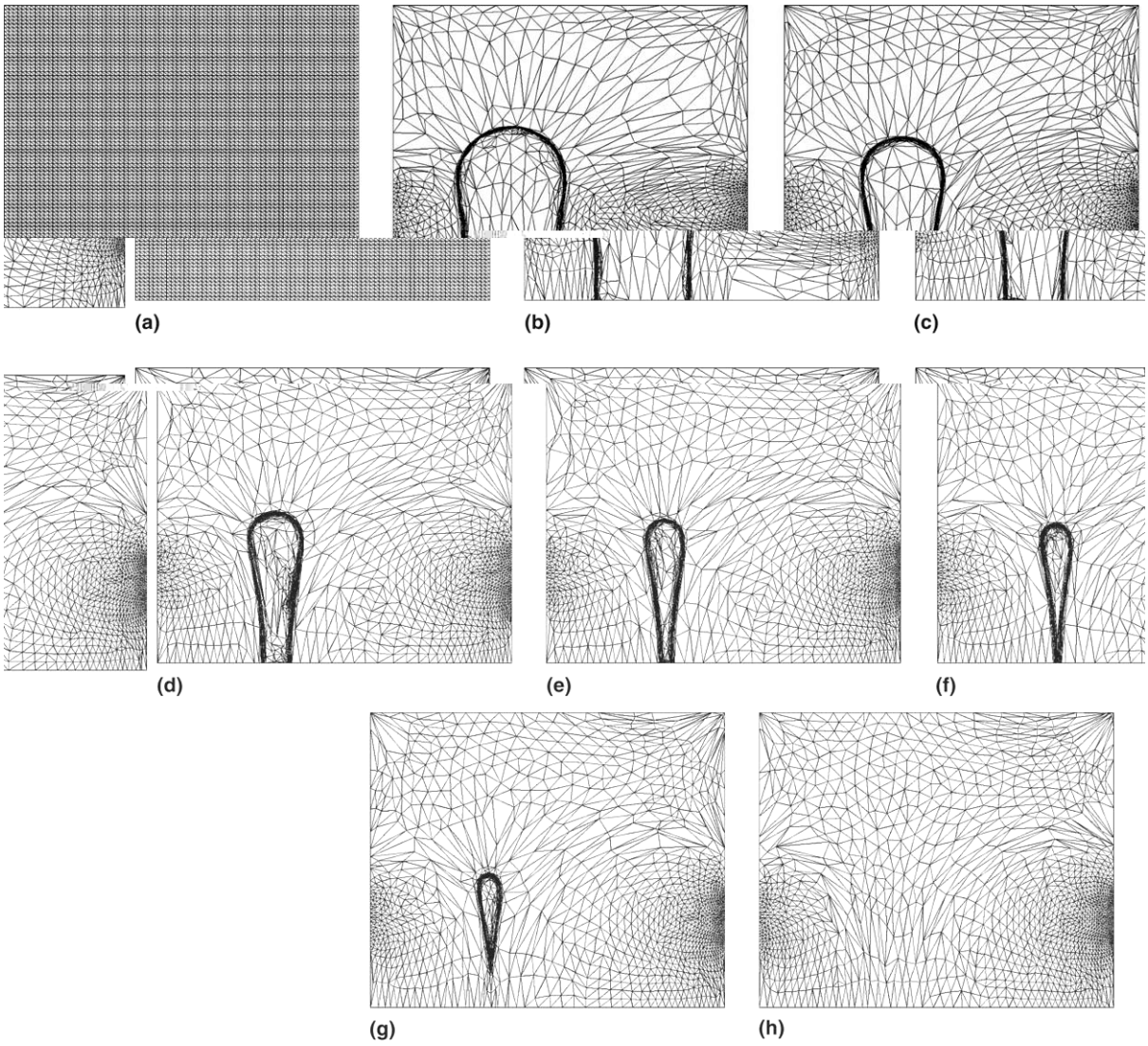

Fig. 17. Formation of a cusp: time-evolution of the mesh. (a) $t = 0$; (b) $t = 0.1$; (c) $t = 0.3$; (d) $t = 0.5$; (e) $t = 0.6$; (f) $t = 0.65$; (g) $t = 0.7$; (h) $t = 1$.

greatly reduced but the position of the interface is still obtained at almost the same position. The temperature variations on the boundaries are however no longer detected. These results are again comparable to those presented in [3,7,11].

6. Conclusions

In this paper a two-equation model for the solution of phase change problems was introduced. In this model, both the temperature T and the phase-field function ϕ are computed. An adaptive remeshing strategy based on a hierarchical error estimator was also described. The presented numerical examples

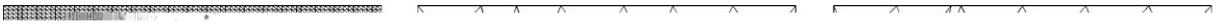

Fig. 18. Formation of a cusp: adaptation on ϕ only. (a) $t = 0$; (b) $t = 0.1$; (c) $t = 0.3$; (d) $t = 0.5$; (e) $t = 0.6$; (f) $t = 0.65$; (g) $t = 0.7$; (h) $t = 1$.

shows that the numerical method coupled with the adaptive strategy provides extremely accurate prediction of both the temperature and interface position.

This finite element method for the Stefan problem described in this paper has been implemented in three dimensions and preliminary results are convincing. The implementation of the hierarchical error estimator is however not yet completed in the three-dimensional case.

Acknowledgements

The authors wish to acknowledge the financial support of NSERC project SKALPEL-ITC.

References

[1] R.E. Bank, A simple analysis of a posteriori error estimates, Appl. Numer. Math. 26 (1998) 153–164.
[2] R.E. Bank, R.K. Smith, A posteriori error estimates based on hierarchical bases, SIAM J. Numer. Anal. 30 (1993) 921–935.
[3] G. Beckett, J.A. Mackenzie, M.L. Robertson, A moving mesh finite element method for the solution of two-dimensional Stefan problems, J. Comput. Phys. 168 (2001) 500–518.
[4] Z. Chen, R.H. Nochetto, A. Schmidt, Error control and adaptivity for a phase relaxation model, Comput. Methods Appl. Mech. Eng. 189 (2000) 249–276.
[5] A. Fortin, Y. Belhamadia, A new enthalpy finite element method for phase change problems, Commun. Numer. Methods Eng. (2003), submitted.
[6] X. Jiang, R.H. Nochetto, A P^1–P^1 finite element method for a phase relaxation model. Part I: Quasi-uniform mesh, SIAM J. Numer. Anal. 35 (3) (1998) 1176–1190.
[7] X. Jiang, R.H. Nochetto, C. Verdi, A P^1–P^1 finite element method for a phase relaxation model. Part II: Adaptively refined meshes, SIAM J. Numer. Anal. 36 (3) (1999) 974–999.
[8] J.A. Mackenzie, M.L. Robertson, The numerical solution of one-dimensional phase change problems using an adaptive moving mesh method, J. Comput. Phys. 161 (2000) 537–557.
[9] J.A. Mackenzie, M.L. Robertson, A moving mesh method for the solution of the one-dimensional phase-field equations, J. Comput. Phys. 181 (2002) 526–544.
[10] F. Ndikumagenge, Estimateur d'erreur a posteriori basé sur une méthode hiérarchique et adaptation de maillage, M.Sc. Thesis, Laval University, 2001.
[11] R.H. Nochetto, M. Paolini, C. Verdi, An adaptive finite element method for two-phase stefan problems in two space dimensions. Part II: Implementation and numerical experiments, SIAM J. Sci. Statist. Comput. 12 (5) (1991) 1207–1244.
[12] R.H. Nochetto, C. Verdi, A. Schmidt, A posteriori error estimation and adaptivity for degenerate parabolic problems, Math. Comput. 69 (2000) 1–24.
[13] D. Pelletier, J. Borggard, J.-F. Hétu, A continuous sensitivity method for conduction and phase change problems, AIAA 2000–0881, Reno, 2000.
[14] É. Pichelin, M. Fortin, S. Boivin, Étude numérique d'estimations d'erreurs a posteriori, REÉF 9 (4) (2000) 467–486.